Linking reduced prefrontal microcircuit inhibition in schizophrenia to EEG biomarkers in silico

Sana Rosanally*[1,2], Frank Mazza*[1,2], Heng Kang Yao[1,2], Etay Hay[1,2,3]

[1]Krembil Centre for Neuroinformatics, Centre for Addiction and Mental Health [2]Department of Physiology, University of Toronto, [3]Department of Psychiatry, University of Toronto, *These authors contributed equally

Abstract

Reduced cortical inhibition by parvalbumin-expressing (PV) interneurons has been associated with impaired cortical processing in the prefrontal cortex (PFC) and altered EEG signals such as oddball mismatch negativity (MMN) in schizophrenia. However, establishing the link between reduced PV interneuron inhibition and reduced MMN experimentally in humans is currently not possible. To overcome these challenges, we used detailed computational models of human PFC microcircuits, and modeled schizophrenia microcircuits by integrating gene-expression data from schizophrenia patients indicating reduced PV interneuron inhibition output and NMDA input. We simulated spiking activity and EEG in microcircuits with different levels of reduced PV interneuron mechanisms and showed that a double effect of the reduction indicated by gene-expression led to a reduced MMN amplitude within the range seen in Schizophrenia patients, whereas a single effect resulted in a smaller decrease in MMN that matched the magnitude seen in patients at high-risk of schizophrenia. In addition, we showed that simulated resting EEG of schizophrenia microcircuits exhibited a right shift from alpha to beta frequencies. Our study thus links the level of reduced PV interneuron inhibition to distinct EEG biomarkers that can serve to better stratify different severities of schizophrenia and improve the early detection using non-invasive brain signals.

Introduction

Cortical dysfunction in schizophrenia involves changes in processing across brain areas [1] and at the cellular and microcircuit level [2–4]. Changes in brain activity underlying schizophrenia may also have signatures in brain signals obtained by electroencephalography (EEG) [1,5], which offer a promising source of objective and quantitative biomarkers [6] that could improve subtyping and early diagnosis, especially when symptoms are mild [7]. However, the link between cellular and microcircuit mechanisms of schizophrenia to cognitive dysfunction and EEG biomarkers remains to be established.

Previous studies indicate that alterations in the microcircuitry of the prefrontal cortex (PFC) may underly impaired cognitive functions in schizophrenia [8–10], particularly those involving inhibitory parvalbumin-expressing (PV) interneurons [11]. PV interneurons provide important and timely inhibition of pyramidal neurons [12], and modulate gamma-frequency (30 - 80 Hz) brain oscillations [13,14] which support cognitive functions in PFC [15] and are reduced in schizophrenia [16,17]. Reduced GABA neurotransmission in the PFC has been associated with altered gamma oscillations and impaired cognition in schizophrenia [18,19]. Accordingly, post-mortem studies found a reduced mRNA expression of PV and GAD67 in PFC PV interneurons in schizophrenia [2,11,20,21]. Studies showed that decreased GAD67 levels in PV interneurons directly influence synaptic inhibition, as GAD67 knock-out in PFC PV interneurons resulted in substantial deficits in inhibition from PV to Pyr neurons in the PFC, which led to increased Pyr neuron excitability and altered excitation/inhibition balance in the microcircuit [22]. Hence, reduced PV expression in PV interneurons in schizophrenia would correspond to reduced synaptic inhibition, which affects the outputs of PV interneurons and may underlie altered microcircuit activity and cognitive impairments. Recent studies also show reduced somatostatin (SST) expression in SST interneurons in schizophrenia [23]. However, SST reduction is seen in a variety of other conditions such as aging and depression [24], whereas PV reduction is indicated as a key mechanism of schizophrenia.

In addition to reduced PV interneuron synaptic inhibition, previous studies indicate that the excitatory innervation onto PV interneurons in the PFC via NMDA receptors is deficient in schizophrenia. Post-mortem studies showed that the NMDA subunit NR2A expression was mostly absent in more than half of PV interneurons in schizophrenia [25–27], whereas there was no

significant change found in other NMDA subunits NR2B-D[28]. NR2A directly affects the potency of glutamate and thus mediates excitatory activity in the NMDA receptors [29]. Furthermore, rodent studies found that working memory depended on NR2A in the PFC as they mediate the majority of evoked NMDA receptor currents in layer 2/3 Pyr neurons [30].

Altered PFC microcircuitry in schizophrenia may underly functional impairments and the respective changes in EEG signals measured during response [31]. Changes in PV interneuron inhibition may lead to detectible changes in EEG signals, since PV interneurons closely modulate inputs to Pyr neurons, which are the main contributors to EEG signals [32]. In particular during the auditory oddball task, which involves the presentation of a series of same-frequency tones followed by a different tone (the deviant tone or "oddball"), schizophrenia patients show a reduced performance and a smaller difference between the PFC EEG signal response to the standard and deviant tones ~100 - 160 ms post-stimulus, referred to as mismatch negativity (MMN) [22]. Recordings of spike activity in monkey auditory cortex and PFC show that the microcircuits in PFC process whether there is a difference between the expected and actual subsequent stimulus and generate a larger spike response for oddball stimuli, which is associated with MMN in the EEG [33]. Studies suggest that the reduced MMN amplitude in schizophrenia is caused by reduced inhibition in the PFC [35], likely involving PV interneurons. In addition to altered EEG during oddball response, studies found changes in resting-state EEG in schizophrenia, such as increased beta power [36–41].

Whereas experimental studies either implicated cellular mechanisms of schizophrenia or characterized changes in EEG features, the link between the two remains to be established in humans due to technical and ethical limitations in probing microcircuitry in the living human brain. Computational models offer a powerful tool for linking altered PV interneuron inhibitory mechanisms in schizophrenia to their EEG biomarkers [42] . While there have been studies that used rat microcircuit models to study mechanisms of EEG in health and disease [26-27], modeling human cortical microcircuits to identify these links is motivated by several reasons. Although there are many circuit and cellular similarities between rodents and humans such as intrinsic firing properties and connectivity patterns between different cell types [44–47], there still remain some important differences. For example, inhibitory synapses from SST and PV interneurons onto Pyr neurons are stronger in humans compared to rodents, have lower synaptic failures and larger postsynaptic potential (PSP) amplitudes [48–50]. Furthermore, there is an significant increased

connection probability between Pyr neurons in human cortical layer 2/3 compared to rodents [51]. In terms of morphology, Pyr neurons are larger in humans and have longer and more complex dendrites which affect input integration [52,53]. The increased availability of human neuronal and synaptic connectivity data [50,51,54] has enabled the generation of detailed models of human cortical microcircuits [55,56]. These constraints can be used to simulate microcircuit activity in health and disease as well as local microcircuit-generated EEG signals, and link microcircuit mechanisms to EEG signatures [55,57,58]. Using models constrained by human data enable predicting effects relevant to human disorders and identifying important clinically-relevant EEG biomarkers in schizophrenia.

In this study, we identified EEG biomarkers of reduced PV interneuron inhibition in models of human PFC microcircuits in schizophrenia, which implemented two key altered PV interneuron mechanisms as estimated from gene expression changes in schizophrenia. We used these models to link reduced PV interneuron inhibition with altered baseline activity and resting EEG in schizophrenia. We then modeled the oddball response as constrained by spike response recorded in monkeys in previous studies, and characterized the effect of reduced PV interneuron inhibition on spiking response and MMN.

Methods

PFC microcircuit models. We modeled detailed human PFC microcircuit models by adapting our previous models of human cortical layer 2/3 microcircuits [55], which consisted of 1000 connected neurons distributed randomly in a 500x500x950 μm^3 volume, situated 250µm - 1200μm below the pia (corresponding to human L2/3) [53]. The neuron models reproduce the firing, dendritic sag current, and synaptic properties measured in human neurons. Four key neuron types were included in the model: Pyr neurons, SST interneurons, PV interneurons, and VIP interneurons [55]. To adapt the models to the human PFC, we applied the neuron type proportions as measured in human PFC tissue, with 72% Pyr neurons and 28% interneurons[59]: 11% PV, 4% SST and 13% VIP interneurons [60]. The models were simulated using NEURON [61], LFPy [58] and parallel computing in high-performance grids (SciNet) [62,63].

PFC baseline activity simulations. We used data recorded in humans and primates to constrain the Pyr neuron baseline activity in the microcircuit models (Human subject 1: 0.66 ± 0.51 Hz,

subject 2: 0.32 ± 0.38 Hz; monkey: 1.31 ± 1.11 Hz) [64]. Target PV interneuron firing rate at baseline was also taken from human and primate single unit recordings (Human subject 1: 2.63 ± 2.55 Hz; monkey: 3.63 ± 4.15 Hz) [64]. The rest of the interneuron activity was constrained using values recorded from rodents *in vivo* (SST: 6.3 ± 0.6 Hz, VIP: 3.7±0.7 Hz) [65]. The microcircuit was injected with background excitatory input, simulated using Ornstein-Uhlenbeck (OU) processes at each dendritic midpoint, to ensure similar levels of inputs along the dendritic path to the soma [66]. We placed 5 additional OU processes along the apical trunk of the Pyr neuron models at 10%, 30%, 50%, 70% and 90% of the apical dendrite length. The base excitatory OU conductance was 28 pS, 280 pS, 30 pS and 66 pS for Pyr, PV, SST and VIP neurons respectively. We did not use inhibitory OU because the model microcircuit provided sufficient inhibition. We scaled the OU conductance values to increase with distance from the soma by multiplying them with the exponent of the relative distance from the soma (ranging from 0 to 1): $\bar{g}_{OU} = \bar{g} \cdot \exp(X_{relative})$.

Schizophrenia microcircuit models. Schizophrenia microcircuits were modelled by altering two types of mechanisms affecting the output and input of PV interneurons. The output mechanism corresponded to a 22% reduction in PV expression in schizophrenia [2], which was modelled by a 22% reduction in synaptic and tonic inhibition from PV interneurons onto other neurons in the microcircuit. The input mechanism corresponded to a 20% decrease in NMDA subunit expression (NR2A) [27], and was modelled by a 20% reduction in NMDA synaptic conductance from Pyr neurons onto PV interneurons. We referred to these schizophrenia microcircuit models as SCZ20, and in addition simulated alternate models of schizophrenia microcircuits (SCZ40) by doubling the effect estimated from expression (44% reduced tonic and synaptic inhibition from PV interneurons and 40% reduced NMDA synaptic conductance from Pyr neurons onto PV interneurons).

Oddball response models. We simulated oddball response using the response firing profile of single neurons in monkey PFC during an oddball auditory task [33]. To reproduce the experimental response (spanning 100 – 160 ms post-stimulus) we used three Pyr neuron activation phases, each consisting of two stimuli with a 10 ms interval. The first activation phase started at 100 ms with 75 Pyr neurons stimulated, followed by a second activation phase at 120 ms with 90 Pyr neurons

stimulated, and a final activation phase at 140 ms of 65 Pyr neurons stimulated to hit a target peak firing rate of 6 Hz, 11 Hz and 7 Hz respectively. All three Pyr neuron activation phases were accompanied by a PV interneuron activation phase preceding the Pyr neuron activation by 5 ms, with 45 PV interneurons stimulated and one stimulus given in each phase.

Simulated microcircuit EEG. We simulated dipole moments together with neuronal spiking activity using LFPy. EEG time series was generated by the microcircuit models using the same methodologies as in previous work [57]. Specifically, we used a four-sphere volume conductor model corresponding to the brain (grey and white matter), cerebrospinal fluid, skull, and scalp with radii of 79 mm, 80 mm, 85 mm, and 90 mm, respectively, that assumes a homogeneous, isotropic, and linear (frequency-independent) conductivity. The conductivity for each sphere was 0.47 S/m, 1.71 S/m, 0.02 S/m, and 0.41 S/m, respectively [67]. The EEG power spectral density was calculated using Welch's method [68] for 3 – 30 Hz using the SciPy python package.

Simulated EEG event related potentials (ERP). To analyze ERP during the oddball MMN response, simulated EEG timeseries were first lowpass filtered to 40 Hz and downsampled to 100 Hz. They were then baseline corrected using the period 0 ms - 500 ms before the stimulus. ERP potential was identified as the largest negative peak from 100 ms – 200 ms post stimulus.

EEG periodic and aperiodic components. We decomposed EEG PSDs into periodic and aperiodic (broadband) components using tools from the FOOOF library [69]. The aperiodic component of the PSD was a 1/f function, defined by a vertical offset and exponent parameter. The periodic components were derived using up to four Gaussians, defined by center frequency (mean), bandwidth (variance) and power (height).

Statistical tests. Statistical significance was determined wherever appropriate using two-sample t-tests. Cohen's *d* was calculated to determine effect size.

Results

We first simulated baseline activity in models of human PFC microcircuits in health and schizophrenia. We modeled healthy microcircuits by adapting our previous detailed models of human cortical L2/3 microcircuits (Fig. 1A-B) using the proportions of Pyr neurons and PV/SST/VIP interneurons in human PFC as seen experimentally (Fig. 1C). To simulate the intrinsic healthy baseline activity of the PFC microcircuit, all neurons received background random excitatory input corresponding to baseline cortical and thalamic inputs. We constrained the baseline microcircuit activity to reproduce firing rates measured *in vivo* in humans (for Pyr and PV interneurons) and rodents (for SST and VIP interneurons). The baseline rates in the different neuron types were - Pyr neuron: 0.73 ± 0.03 Hz, SST: 3.64 ± 0.14 Hz, PV: 6.64 ± 0.17 Hz, VIP: 2.51 ± 0.14 Hz (Fig. 1D). We analyzed the spectral power of the microcircuit activity by simulating EEG during baseline activity and calculating the PSD. The simulated PSD exhibited a peak in the theta (4 – 8 Hz) and alpha (8 – 12 Hz) frequency bands (Fig. 1E), as well as a 1/f relationship, all of which were in line with spectral properties of human prefrontal resting-state EEG activity.

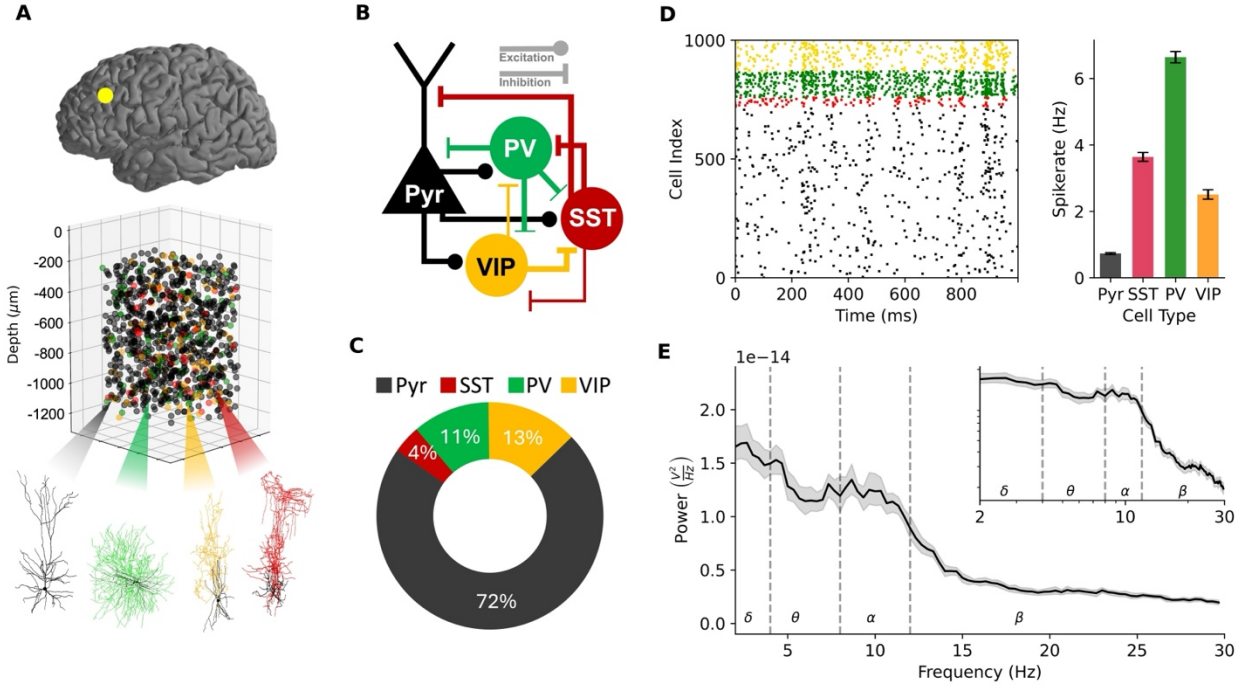

Figure 1. Detailed models of human prefrontal microcircuit baseline spiking activity and EEG. (A) Detailed models of human PFC microcircuits showing placement of 1000 connected neurons, human neuronal morphologies of the four key neuron types (green: PV, red: SST, black; Pyr, yellow: VIP), and the media from the microcircuit to the scalp EEG electrode. **(B)** Connectivity diagram between neuron types in the microcircuit. **(C)** Cellular proportions of each neuron type: Pyr (72%), SST (4%), PV (11%), VIP (13%). **(D)** Left - raster plot of neuronal spiking in the microcircuit at baseline, color-coded according

to each neuron type. Right - baseline firing rates of all neurons (mean and SD). **(E)** Power spectral density (PSD) plot of simulated EEG at baseline (mean across n = 30 random microcircuits, showing bootstrap mean and 95% confidence interval. Canonical frequency bands are shown by vertical dotted lines. Inset: the same plot in logarithmic axes scale, showing 1/f relationship.

We modelled microcircuit changes in schizophrenia by implementing two key mechanisms involving PV interneuron inhibition (Fig. 2A) according to human PFC post-mortem studies. The first mechanism (referred to as the output mechanism) was a reduced PV interneuron synaptic and tonic inhibition conductance, either at the level estimated from expression (22%, SCZ20) or the double effect (44%, SCZ40). The second mechanism (referred to as the input mechanism) was a reduction in NMDA synaptic conductance from Pyr neurons to PV interneurons, either at the level estimated from expression (20%, SCZ20) or double the effect (40%, SCZ40) model.

We simulated baseline activity in the schizophrenia microcircuits and compared it to healthy microcircuits (Fig. 2B). Baseline Pyr neuron firing rates in the SCZ20 microcircuit model (0.87 ± 0.03 Hz) and the SCZ40 microcircuit model (1.18 ± 0.04 Hz) increased by 20% ($p < 0.0005$, Cohen's $d = 4.8$) and 62% ($p < 0.0005$, Cohen's $d = 12.8$) respectively compared to the healthy microcircuit (0.73 ± 0.03 Hz). Simulation of either the input or output mechanisms alone showed that the SCZ_{Input} mechanism was the main contributor to the effect on the baseline Pyr neuron firing rate ($SCZ20_{Input}$ +18%, 0.86 ± 0.03 Hz, $p < 0.0005$, Cohen's $d = 4.3$; $SCZ40_{Input}$: +46%, 1.07 ± 0.05 Hz, $p < 0.0005$, Cohen's $d = 8.1$), whereas the SCZ_{Output} mechanism had a minor effect ($SCZ20_{Output}$: +3%, 0.75 ± 0.03 Hz, $p = 0.002$, Cohen's $d = 0.8$; $SCZ40_{Output}$: +10%, 0.80 ± 0.03 Hz, $p < 0.0005$, Cohen's $d = 2.41$).

Interneuron baseline firing rates also increased in schizophrenia microcircuits (Fig. 2C). PV interneuron firing rates increased by 22% in SCZ20 (8.09 ± 0.21 Hz, $p < 0.0005$, Cohen's $d = 7.5$), and by 66% in SCZ40 (11.05 ± 0.28 Hz, $p < 0.0005$, Cohen's $d = 18.8$), SST interneuron firing rates increased by 19% in SCZ20 (4.33 ± 0.13 Hz, $p < 0.0005$, Cohen's $d = 5.1$) and by 52% in SCZ40 (5.53 ± 0.19 Hz, $p < 0.0005$, Cohen's $d = 11.1$), and VIP interneuron firing rates increased by 40% in SCZ20 (3.5 ± 0.19 Hz, $p < 0.0005$, Cohen's $d = 5.9$) and by 120% in SCZ40 (5.51 ± 0.24 Hz, $p < 0.0005$, $d = 15.0$).

The SCZ_{Output} mechanism had a larger effect on PV interneuron firing rates compared to the SCZ_{Input} mechanism (+51%, 10.05 ± 0.25 Hz, $p < 0.0005$, Cohen's $d = 15.7$ vs 10% increase, 7.27 ± 0.21 Hz, $p < 0.0005$, Cohen's $d = 3.2$, respectively in SCZ40, Fig. 2D). In contrast, for the other interneurons the SCZ_{Input} mechanism had a larger effect than the SCZ_{Output} mechanism (SST in SCZ40: 39% increase, 5.06 ± 0.19 Hz, $p < 0.0005$, Cohen's $d = 8.4$ vs 8% increase, 3.94 ± 0.11 Hz, $p < 0.0005$, Cohen's $d = 2.4$; VIP in SCZ40: 73% increase, 4.33 ± 0.28 Hz, $p < 0.0005$, Cohen's $d = 8.0$ vs 32% increase, 3.31 ± 0.18 Hz, $p < 0.0005$, Cohen's $d = 4.9$, respectively).

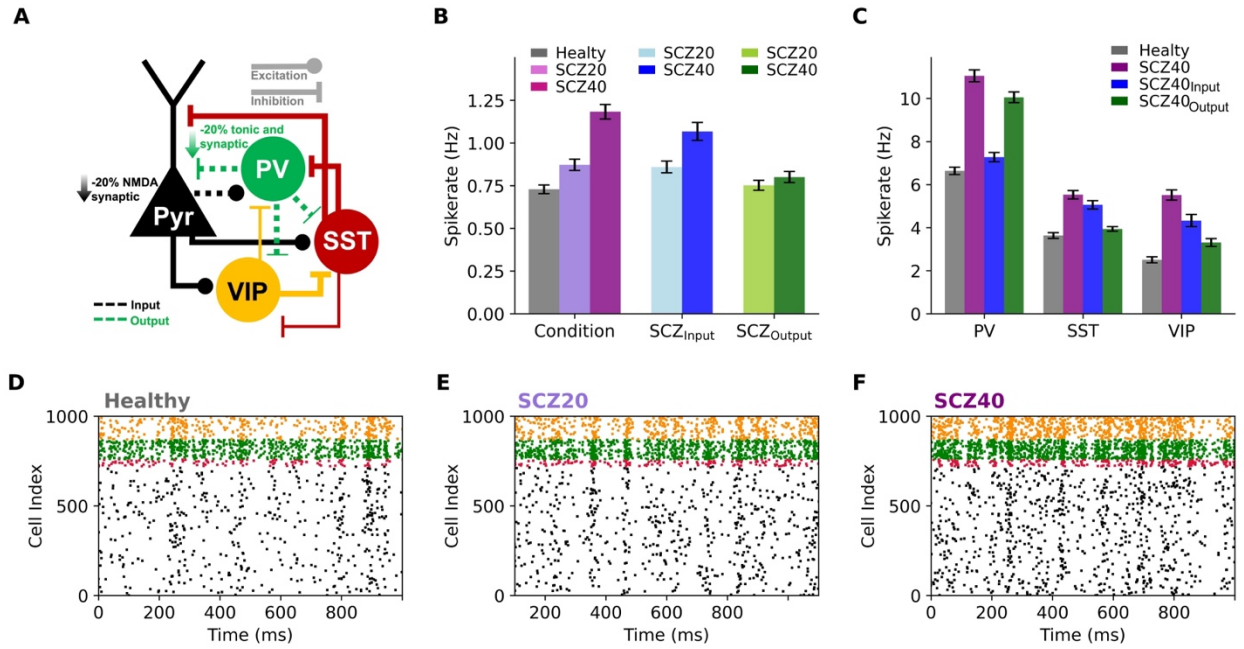

Figure 2: Increased baseline activity in models of schizophrenia cortical microcircuits with altered PV interneuron inhibition. (A) Connectivity diagram of the schizophrenia microcircuit models showing the altered PV output and input mechanisms (green and black dashed lines). **(B)** Pyr baseline spike rates in healthy, SCZ20 and SCZ40 microcircuits, and in microcircuits that included only the SCZ_{Input} or SCZ_{Output} mechanism (mean and SD). **(C)** Baseline interneuron spike rates in healthy, SCZ40 and microcircuits that included only the $SCZ40_{Input}$ or $SCZ40_{Output}$ mechanism (mean and SD). **(D)** Raster plot of example spiking activity in a healthy microcircuit. **(E)** Same as (D) but for a SCZ20 microcircuit. **(F)** Same as (D) but for a SCZ40 microcircuit.

We looked for signatures of the altered inhibition effects on simulated resting-state EEG by comparing the PSD in healthy and schizophrenia microcircuit models (n = 30 randomized microcircuits, Fig. 3). Simulated EEG from schizophrenia microcircuits showed a prominent peak in the alpha band (8 - 12 Hz) as the healthy microcircuit models but exhibited a rightward shift (Fig. 3A). We decomposed the EEG PSDs into aperiodic (Fig. 3B) and periodic (Fig. 3C)

components to compare the distinct functional components of absolute PSDs. There were no major changes in aperiodic broadband power (Fig. 3B), but there was a large rightward shift in periodic peak alpha frequency from 10.1 to 12.4 Hz in SCZ40 compared to healthy (+23%, $p < 0.0005$, Cohen's $d = 1.5$, Fig. 3C), evident also in a large increase in low beta (12 – 20 Hz) power compared to healthy (+63%, $p < 0.0005$, Cohen's $d = 4.78$). There was also a small rightward shift in peak alpha frequency from 10.1 to 11.2 Hz in SCZ20 compared to healthy (+11%, $p = 0.001$, Cohen's $d = 0.8$).

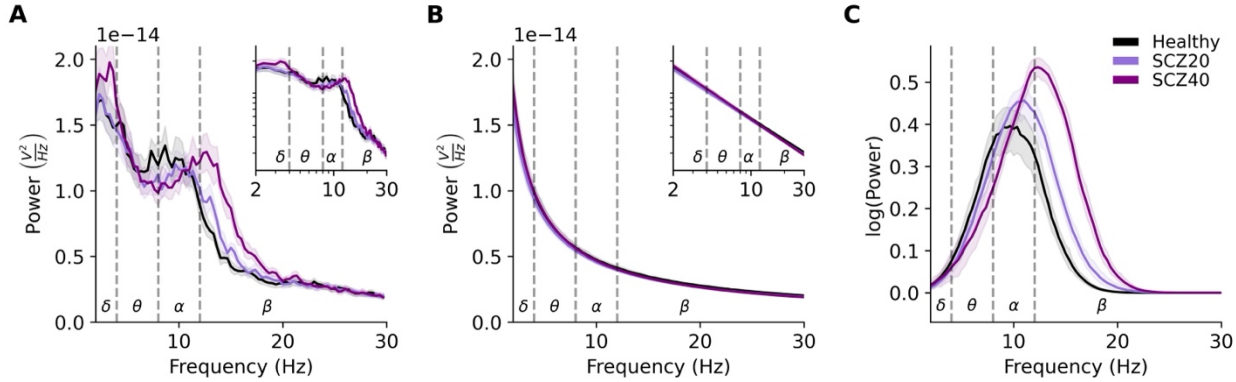

Figure 3: Resting-state EEG signatures of reduced PV interneuron inhibition in schizophrenia microcircuit models. (**A)** Power spectral density plot of simulated EEG from the healthy (black), SCZ20 (magenta) and SCZ40 (purple) microcircuit models (n = 30 randomized microcircuits per condition, bootstrapped mean and 95% confidence interval). (**B)** Aperiodic component of the PSD in the different conditions. (**C)** Periodic component of the PSD in the different conditions.

After modelling the baseline activity, which in the PFC also corresponded to the activity during response to standard tones, we simulated oddball (deviant tone) response by reproducing the firing rate profile of Pyr neurons along the period 100 – 160 ms post-stimulus as recorded in primates (Fig. 4A,B). We then applied the same stimulus paradigm to the SCZ20 and SCZ40 microcircuit models. Reduced PV interneuron inhibition had only a small effect on Pyr neuron response in SCZ20 microcircuits (Fig. 4C, healthy: 6.85 ± 0.4 Hz; SCZ20: +3%, 7.04 ± 0.39 Hz $p = 0.008$, Cohen's $d = 0.5$) and a slightly larger effect in SCZ40 microcircuits (+9%, 7.46 ± 0.46 Hz, $p < 0.0005$, Cohen's $d = 1.4$).

To better understand the implications of a larger increase in baseline (standard response) PFC firing compared to oddball response in schizophrenia microcircuits, we calculated the signal-to-noise ratio (SNR) of oddball/standard response firing rates. The SNR ratio decreased by 15%

in SCZ20 microcircuits (healthy: 8.69 ± 0.75, SCZ20: 7.39 ± 0.56, $p < 0.0005$, Cohen's $d = 1.0$, Fig. 4D), and by 31% in SCZ40 microcircuits (6.04 ± 0.54, $p < 0.0005$, Cohen's $d = 4.1$, Fig. 4D).

We next compared the MMN in the ERP response in healthy and schizophrenia microcircuit models (Fig. 4E,F), by simulating EEG during response and baseline and plotting the difference. The MMN response in schizophrenia microcircuits was significantly reduced compared to healthy microcircuit, with a 16% decrease in peak amplitude in SCZ20 microcircuits (healthy: 4.43 ± 0.4 pV, SCZ20: 3.7 ± 0.4 pV, $p < 0.0005$, Cohen's $d = 1.6$, Fig. 4F), and a 32% decrease in peak amplitude in SCZ40 microcircuits (3.0 ± 0.5 pV, $p < 0.0005$, Cohen's $d = 3.1$, Fig. 4F).

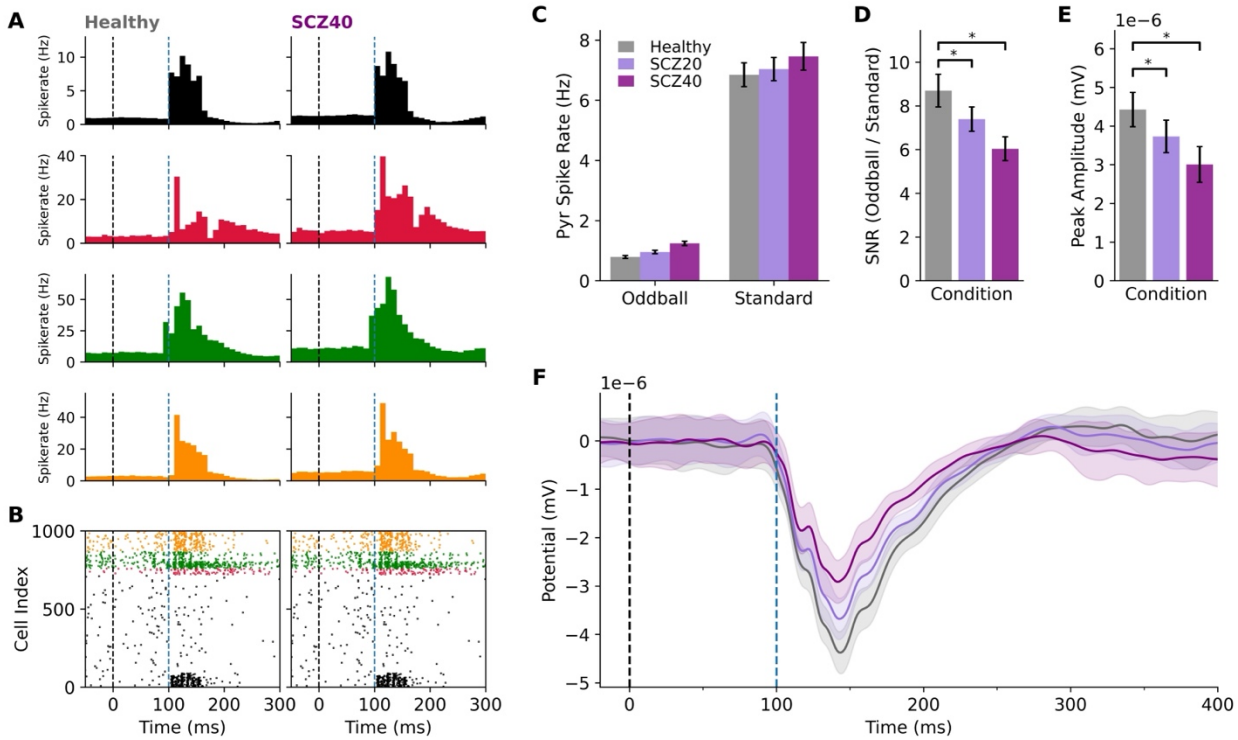

Figure 4: Simulated oddball response and MMN in healthy and schizophrenia microcircuits. (A) Peristimulus time histogram (n = 100 randomized microcircuits) of simulated oddball response in healthy (left) vs. SCZ40 (right) microcircuit models. Healthy models reproduced response firing rates and profiles as recorded in primates. Blue dashed line denotes the external stimulus time and red dashed line denotes PFC activation time. **(B)** Raster plot of simulated spike response in healthy (left) and schizophrenia (right) microcircuit models. **(C)** Average Pyr spike rate during simulated standard (baseline) and oddball response in healthy, SCZ20 and SCZ40 microcircuits (mean and SD). (**D)** SNR of Pyr neurons in healthy, SCZ20 and SCZ40 microcircuits (mean and SD). Asterisks indicate significance $p < 0.05$. **(E)** Simulated ERP of the MMN during oddball response of healthy, SCZ20, and SCZ40 microcircuit models (oddball - standard response, mean and SD) (**F**) Peak amplitude of MMN response in healthy, SCZ20 and SCZ40 microcircuits (mean and SD). Asterisks indicate significance $p < 0.05$.

Discussion

We determined the implications of reduced PV interneuron inhibition in schizophrenia on impaired processing in prefrontal cortical microcircuits and the associated EEG signatures, using detailed models constrained by human cellular, circuit and gene-expression data in health and schizophrenia. Our simulations of microcircuit baseline activity and oddball response showed that a reduced PV interneuron inhibition in schizophrenia can account for the decrease in MMN amplitude seen in patients, by increasing baseline spike rates (noise) and thus decreasing the SNR of cortical processing of oddball vs standard response. Our results thus mechanistically link altered cell-specific inhibition with clinically relevant EEG changes in schizophrenia, establishing PV interneuron inhibition as a target mechanism for new treatments. Moreover, our results make testable quantitative predictions about the degree of reduced PV inhibition that underlies reduced MMN amplitude in different severities, which may improve the subtyping of schizophrenia and the early detection of the disorder when it is still largely asymptomatic.

Reduced MMN amplitude in our simulated schizophrenia microcircuits is in agreement with previous clinical studies in patients [70,71]. Our results mechanistically link the reduced MMN amplitude with reduced PV interneuron inhibition, and thus validate previous hypotheses [72]. The reduction in MMN amplitude of 33% on average in our SCZ40 microcircuits is within the range seen in schizophrenia patients [70,71]. It involved a double effect of the percent indicated by gene expression, which is supported by other gene expression studies that found a larger reduction in PV expression in bulk cortical layers 3 and 4 [2] than the reduction estimated on average in PV interneurons. The SCZ40 effect on MMN amplitude was about twice the effect of the SCZ20, which indicate a linear relationship. The dysfunction in NMDA mechanism contributed more than the reduced synaptic conductance, suggesting that altered MMN amplitude deficits may primarily result from NMDA receptor dysfunction, which has been associated with both MMN amplitude reductions [73] and psychotic symptoms [74]. According to a recent meta-analysis review, the MMN signal was found to be the ERP measure that best predicted the conversion to psychosis in clinically-high-risk patients [71].

The decrease in MMN amplitude of 16% on average in our SCZ20 models corresponds well with the 15% decrease seen on average in individuals that are at clinically high risk for schizophrenia [7,75]. This indicates that the at-risk population may already have a reduced PV interneuron inhibition, which may underly the milder symptoms that could later develop into

schizophrenia. For example, people at high-risk of developing schizophrenia have a reduced ability to distinguish novel features of the environment from their background at early stages of cognitive processing. This could predispose the individual to schizophrenia symptoms such as misinterpretations of one's surroundings, perceptual illusions or the experience of ordinary stimuli as intense, distracting or salient [75]. Thus, our models of schizophrenia PFC microcircuits quantitatively characterize the implications of different levels of reduced PV interneuron inhibition on the MMN response, which may be used to better stratify schizophrenia subtypes and severity, and improve the early detection and outcome prediction in at-risk population.

The MMN amplitude was reduced in schizophrenia microcircuits, but Pyr neuron firing rates at baseline and oddball response increased. A possible explanation is that reduction in PV interneuron inhibition disinhibited SST interneurons, enhancing their inhibition of the distal apical dendrites of Pyr neurons [76], thus reducing the summated potential amplitude recorded by EEG [77]. The apical dendrites generally receive a large number of excitatory inputs from cortical areas as well as globally modulatory subcortical projections, making the apical region a negative current source. Since the distance between the apical dendrites source and the soma and basal dendrites sink is large, this difference in potential is the major contributor of the dipole from the neuron. Increased SST interneuron inhibition of the apical dendrites due to the reduced in PV interneuron inhibition makes the apical dendrites less positively charged, which consequently reduces the electric dipole of the neuron and thus the MMN amplitude measured by EEG.

The increased baseline firing rates in schizophrenia microcircuits across all cell types are the net effect of different circuit interactions resulting from the reduced PV interneuron inhibition. PV interneurons innervate the peri-somatic region of Pyr neurons (soma and basal dendrites) and thus have a powerful regulatory control over Pyr neuron activity. Hence, a reduction of PV interneuron inhibition will ultimately disinhibit the nearby Pyr excitatory neurons, causing them to be more excited and fire at a higher rate. In turn, the increased Pyr neuron rates can account for the increased rates of interneurons, since they all receive excitatory input from Pyr neurons. The smaller increase in SST interneuron firing rate in our simulations is likely due to SST interneurons being more strongly inhibited by both PV and VIP interneurons, whereas PV interneurons are primarily inhibited by VIP interneurons. As part of the net effect of reduced PV interneuron inhibition, the increased activity of VIP interneurons keeps the microcircuit from being overinhibited by the increased activity in PV and SST interneurons. The increase in baseline rates

is in agreement with previous studies that showed increased baseline activity in schizophrenia, which has been associated with positive symptoms [78,79].

Our results show that the reduced NMDA input mechanism of PV interneurons in schizophrenia had a larger contribution to the increased Pyr neuron baseline firing rate compared to the reduced synaptic/tonic output mechanism. This was likely because the reduced NMDA input conductance directly reduced the firing rates of PV interneurons, thus completely abolishing the resulting IPSPs, whereas the reduced synaptic/tonic output mechanism involved only a partial reduction of the IPSP amplitude.

The schizophrenia microcircuit models exhibited a rightward shift in the peak frequency from high-alpha band to low-beta band. These results agree with numerous studies that reported an increase in resting-state beta power in schizophrenia [36–41]. Reduced power in the alpha frequency band has been associated with schizophrenia positive and negative symptoms and with chronicity [80]. Beta oscillations are observed during executive control of action [81–83], working memory [84,85] and thus increased beta power is associated with increased distraction [86,87], which is seen in schizophrenia. Other PSD changes that we did not capture in the models, such as increased theta power, could be due to additional mechanisms that change in schizophrenia, especially a loss of SST interneuron inhibition as suggested by recent gene expression studies [3,23,87,88].

Our biomarkers can be applied on patient data, with simulation of additional levels of PV inhibition reduction, to better stratify patients and facilitate early detection in at-risk population. Our models can also serve to identify EEG biomarkers of other mechanisms of schizophrenia, e.g. the possible altered levels of SST interneuron inhibition indicated by our study and recent gene-expression studies [3,23,89]. Moreover, the computational models that we developed can provide a powerful tool to identify potential EEG biomarkers of novel therapeutic compounds and treatments for schizophrenia via *in-silico* testing to improve monitoring treatment efficacy and dose prediction [90]. The simulated EEG that our models provide can also be related to that of recorded EEG, by scaling to account for the difference between the number of neurons in our models compared to the amount of neurons that generate the recorded EEG at a given electrode, which would be about a factor of 10,000 to 100,000 [91,92].

In this study, we applied gene expression data to estimate a reduction in synaptic and tonic conductance due to inhibitory connections from PV interneurons [2]. The link between gene

expression and cellular function is not trivial, but a few factors support our framework. Studies have shown that in schizophrenia, interneurons exhibited reduced PV accompanied with reduced GAD67, an enzyme that synthesizes GABA [93]. Moreover, a reduction of cortical PV-expressing GABAergic interneurons was shown to elicit deficits in social behaviour and cognition [94]. The change in gene expression could alternatively correspond to a reduced number of synapses [95], however the net decrease in inhibition would be mostly similar in either scenario. We also simplified the implementation of the 50% reduction in NMDA NR2A subunit, which is expressed in 40% of the PV interneurons in the PFC [27], as a 20% reduction in overall synaptic NMDA conductance from all Pyr → PV interneurons in the microcircuit, assuming that the net decrease in inhibition would be mostly similar in either case.

For both NMDA and synaptic mechanisms, we examined an implementation that was of the proportion indicated by the change in gene expression (SCZ20), as well as an alternative implementation that involved a double effect (SCZ40). The correspondence of the reduction in MMN amplitude seen experimentally in schizophrenia and the simulated MMN in microcircuit models with the double effect (SCZ40) suggest that the percent change in gene expression may translate to a larger physiological effect in terms of NMDA and synaptic conductance. Although additional mechanisms could explain the discrepancy, a doubling effect of the magnitude indicated by altered expression is possible. Alternatively, bulk-tissue expression studies indicate that some layers (3 and 4) may involve a larger reduction of PV expression than suggested by average expression per PV interneurons [2]. Future studies should therefore characterize the expression in layer 2/3 PV interneurons to improve the estimate.

Our models were constrained with microcircuit data taken from PFC where possible, and various other brain regions due to limited availability of human neuronal and microcircuit data, thus the models aimed to primarily represent canonical cortical microcircuits. While different brain regions such as the PFC and sensory regions have some differences in wiring and function when taking into account all six layers of the cortex, the canonical layers 2 and 3 microcircuitry is similar across regions [96]. Finally, for this study we modelled oddball processing in a single region (PFC microcircuit) rather than the interaction between multiple brain regions. While oddball processing may involve ongoing interactions between PFC and other brain regions such as the primary and secondary auditory cortex [97], the main computation of the MMN signal is performed in the PFC [33], thus supporting modeling and studying it in isolation. However, future studies can simulate

multiple microcircuits to study the multi-regional aspects of oddball processing in health and schizophrenia.

Acknowledgements

SR, FM, HKY and EH thank the Krembil Foundation for funding support. FM and HKY were also supported by the Ontario Graduate Scholarship and by a stipend award from the Department of Physiology at University of Toronto.

References

1. Weber LA, Diaconescu AO, Mathys C, Schmidt A, Kometer M, Vollenweider F, et al. Ketamine Affects Prediction Errors about Statistical Regularities: A Computational Single-Trial Analysis of the Mismatch Negativity. J Neurosci. 2020;40: 5658–5668. doi:10.1523/JNEUROSCI.3069-19.2020

2. Hashimoto T, Volk DW, Eggan SM, Mirnics K, Pierri JN, Sun Z, et al. Gene Expression Deficits in a Subclass of GABA Neurons in the Prefrontal Cortex of Subjects with Schizophrenia. J Neurosci. 2003;23: 6315–6326. doi:10.1523/JNEUROSCI.23-15-06315.2003

3. Hashimoto T, Bazmi HH, Mirnics K, Wu Q, Sampson AR, Lewis DA. Conserved regional patterns of GABA-related transcript expression in the neocortex of subjects with schizophrenia. Am J Psychiatry. 2008;165: 479–489. doi:10.1176/appi.ajp.2007.07081223

4. Lewis DA, Gonzalez-Burgos G. Intrinsic excitatory connections in the prefrontal cortex and the pathophysiology of schizophrenia. Brain Res Bull. 2000;52: 309–317. doi:10.1016/S0361-9230(99)00243-9

5. Avissar M, Xie S, Vail B, Lopez-Calderon J, Wang Y, Javitt DC. Meta-analysis of mismatch negativity to simple versus complex deviants in schizophrenia. Schizophr Res. 2018;191: 25–34. doi:10.1016/j.schres.2017.07.009

6. Sun J, Cao R, Zhou M, Hussain W, Wang B, Xue J, et al. A hybrid deep neural network for classification of schizophrenia using EEG Data. Sci Rep. 2021;11: 4706. doi:10.1038/s41598-021-83350-6

7. Charlton CE, Lepock JR, Hauke DJ, Mizrahi R, Kiang M, Diaconescu AO. Atypical prediction error learning is associated with prodromal symptoms in individuals at clinical high risk for psychosis. Schizophrenia. 2022;8: 1–10. doi:10.1038/s41537-022-00302-3

8. Weinberger DR, Berman KF, Zec RF. Physiologic dysfunction of dorsolateral prefrontal cortex in schizophrenia. I. Regional cerebral blood flow evidence. Arch Gen Psychiatry. 1986;43: 114–124. doi:10.1001/archpsyc.1986.01800020020004

9. Goldman-Rakic PS. Working memory dysfunction in schizophrenia. J Neuropsychiatry Clin Neurosci. 1994;6: 348–357. doi:10.1176/jnp.6.4.348

10. Lewis DA, Lieberman JA. Catching up on schizophrenia: natural history and neurobiology. Neuron. 2000;28: 325–334. doi:10.1016/s0896-6273(00)00111-2

11. Rao SG, Williams GV, Goldman-Rakic PS. Destruction and creation of spatial tuning by disinhibition: GABA(A) blockade of prefrontal cortical neurons engaged by working memory. J Neurosci Off J Soc Neurosci. 2000;20: 485–494.

12. Gonzalez-Burgos G, Lewis DA. GABA neurons and the mechanisms of network oscillations: implications for understanding cortical dysfunction in schizophrenia. Schizophr Bull. 2008;34: 944–961. doi:10.1093/schbul/sbn070

13. Cardin JA, Carlén M, Meletis K, Knoblich U, Zhang F, Deisseroth K, et al. Driving fast-spiking cells induces gamma rhythm and controls sensory responses. Nature. 2009;459: 663–667. doi:10.1038/nature08002

14. Sohal VS, Zhang F, Yizhar O, Deisseroth K. Parvalbumin neurons and gamma rhythms enhance cortical circuit performance. Nature. 2009;459: 698–702. doi:10.1038/nature07991

15. Lewis DA, Curley AA, Glausier JR, Volk DW. Cortical parvalbumin interneurons and cognitive dysfunction in schizophrenia. Trends Neurosci. 2012;35: 57–67. doi:10.1016/j.tins.2011.10.004

16. Cho RY, Konecky RO, Carter CS. Impairments in frontal cortical gamma synchrony and cognitive control in schizophrenia. Proc Natl Acad Sci U S A. 2006;103: 19878–19883. doi:10.1073/pnas.0609440103

17. Minzenberg MJ, Firl AJ, Yoon JH, Gomes GC, Reinking C, Carter CS. Gamma oscillatory power is impaired during cognitive control independent of medication status in first-episode schizophrenia. Neuropsychopharmacol Off Publ Am Coll Neuropsychopharmacol. 2010;35: 2590–2599. doi:10.1038/npp.2010.150

18. Lewis DA, Hashimoto T, Volk DW. Cortical inhibitory neurons and schizophrenia. Nat Rev Neurosci. 2005;6: 312–324. doi:10.1038/nrn1648

19. Gonzalez-Burgos G, Hashimoto T, Lewis DA. Alterations of Cortical GABA Neurons and Network Oscillations in Schizophrenia. Curr Psychiatry Rep. 2010;12: 335–344. doi:10.1007/s11920-010-0124-8

20. Curley AA, Arion D, Volk DW, Asafu-Adjei JK, Sampson AR, Fish KN, et al. Cortical Deficits of Glutamic Acid Decarboxylase 67 Expression in Schizophrenia: Clinical, Protein,

and Cell Type-Specific Features. Am J Psychiatry. 2011;168: 921–929. doi:10.1176/appi.ajp.2011.11010052

21. Toker L, Mancarci BO, Tripathy S, Pavlidis P. Transcriptomic evidence for alterations in astrocytes and parvalbumin interneurons in bipolar disorder and schizophrenia subjects. Biol Psychiatry. 2018;84: 787–796. doi:10.1016/j.biopsych.2018.07.010

22. Lazarus MS, Krishnan K, Huang ZJ. GAD67 Deficiency in Parvalbumin Interneurons Produces Deficits in Inhibitory Transmission and Network Disinhibition in Mouse Prefrontal Cortex. Cereb Cortex N Y NY. 2015;25: 1290–1296. doi:10.1093/cercor/bht322

23. Dienel SJ, Fish KN, Lewis DA. The Nature of Prefrontal Cortical GABA Neuron Alterations in Schizophrenia: Markedly Lower Somatostatin and Parvalbumin Gene Expression Without Missing Neurons. Am J Psychiatry. 2023; appiajp20220676. doi:10.1176/appi.ajp.20220676

24. Sibille E. Reduced Somatostatin Expression or Somatostatin-Positive Gamma-Aminobutyric Acid Neurons: A Shared Pathology Across Brain Disorders. Biol Psychiatry. 2017;81: 467–469. doi:10.1016/j.biopsych.2016.12.002

25. Woo T-UW, Walsh JP, Benes FM. Density of glutamic acid decarboxylase 67 messenger RNA-containing neurons that express the N-methyl-D-aspartate receptor subunit NR2A in the anterior cingulate cortex in schizophrenia and bipolar disorder. Arch Gen Psychiatry. 2004;61: 649–657. doi:10.1001/archpsyc.61.7.649

26. Woo T-UW, Kim AM, Viscidi E. DISEASE-SPECIFIC ALTERATIONS IN GLUTAMATERGIC NEUROTRANSMISSION ON INHIBITORY INTERNEURONS IN THE PREFRONTAL CORTEX IN SCHIZOPHRENIA. Brain Res. 2008;1218: 267–277. doi:10.1016/j.brainres.2008.03.092

27. Bitanihirwe B, Lim M, Kelley J, Kaneko T, Woo T. Glutamatergic deficits and parvalbumin-containing inhibitory neurons in the prefrontal cortex in schizophrenia. BMC Psychiatry. 2009;9: 71. doi:10.1186/1471-244X-9-71

28. Akbarian S, Sucher NJ, Bradley D, Tafazzoli A, Trinh D, Hetrick WP, et al. Selective alterations in gene expression for NMDA receptor subunits in prefrontal cortex of schizophrenics. J Neurosci Off J Soc Neurosci. 1996;16: 19–30. doi:10.1523/JNEUROSCI.16-01-00019.1996

29. Anson LC, Chen PE, Wyllie DJA, Colquhoun D, Schoepfer R. Identification of Amino Acid Residues of the NR2A Subunit That Control Glutamate Potency in Recombinant NR1/NR2A NMDA Receptors. J Neurosci. 1998;18: 581–589. doi:10.1523/JNEUROSCI.18-02-00581.1998

30. McQuail JA, Beas BS, Kelly KB, Simpson KL, Frazier CJ, Setlow B, et al. NR2A-Containing NMDARs in the Prefrontal Cortex Are Required for Working Memory and Associated with Age-Related Cognitive Decline. J Neurosci. 2016;36: 12537–12548. doi:10.1523/JNEUROSCI.2332-16.2016

31. Karlsgodt KH, Sun D, Cannon TD. Structural and Functional Brain Abnormalities in Schizophrenia. Curr Dir Psychol Sci. 2010;19: 226–231. doi:10.1177/0963721410377601

32. Kirschstein T, Köhling R. What is the source of the EEG? Clin EEG Neurosci. 2009;40: 146–149. doi:10.1177/155005940904000305

33. Camalier CR, Scarim KC, Mishkin M, Averbeck BB. A comparison of auditory oddball responses in dorsolateral prefrontal cortex, basolateral amygdala and auditory cortex of macaque. J Cogn Neurosci. 2019;31: 1054–1064. doi:10.1162/jocn_a_01387

34. Schmidt A, Diaconescu AO, Kometer M, Friston KJ, Stephan KE, Vollenweider FX. Modeling ketamine effects on synaptic plasticity during the mismatch negativity. Cereb Cortex N Y N 1991. 2013;23: 2394–2406. doi:10.1093/cercor/bhs238

35. Fung SJ, Webster MJ, Sivagnanasundaram S, Duncan C, Elashoff M, Weickert CS. Expression of interneuron markers in the dorsolateral prefrontal cortex of the developing human and in schizophrenia. Am J Psychiatry. 2010;167: 1479–1488. doi:10.1176/appi.ajp.2010.09060784

36. Begić D, Popović-Knapić V, Grubišin J, Kosanović-Rajačić B, Filipčić I, Telarović I, et al. Quantitative electroencephalography in schizophrenia and depression. Psychiatr Danub. 2011;23: 355–362.

37. Kemali D, Galderisi S, Maj M, Mucci A, Gregorio MD, Bucci P. Computerized EEG topography findings in schizophrenic patients before and after haloperidol treatment. Int J Psychophysiol. 1992;13: 283–290. doi:10.1016/0167-8760(92)90078-P

38. Galderisi S, Mucci A, Mignone ML, Maj M, Kemali D. CEEG mapping in drug-free schizophrenics: Differences from healthy subjects and changes induced by haloperidol treatment. Schizophr Res. 1991;6: 15–23. doi:10.1016/0920-9964(91)90016-K

39. Boutros NN, Arfken C, Galderisi S, Warrick J, Pratt G, Iacono W. The Status of Spectral EEG Abnormality as a Diagnostic Test for Schizophrenia. Schizophr Res. 2008;99: 225–237. doi:10.1016/j.schres.2007.11.020

40. Venables NC, Bernat EM, Sponheim SR. Genetic and Disorder-Specific Aspects of Resting State EEG Abnormalities in Schizophrenia. Schizophr Bull. 2009;35: 826–839. doi:10.1093/schbul/sbn021

41. Narayanan B, O'Neil K, Berwise C, Stevens MC, Calhoun VD, Clementz BA, et al. Resting state electroencephalogram oscillatory abnormalities in schizophrenia and psychotic bipolar patients and their relatives from the bipolar and schizophrenia network on intermediate phenotypes study. Biol Psychiatry. 2014;76: 456–465. doi:10.1016/j.biopsych.2013.12.008

42. Mäki-Marttunen T, Krull F, Bettella F, Hagen E, Næss S, Ness TV, et al. Alterations in Schizophrenia-Associated Genes Can Lead to Increased Power in Delta Oscillations. Cereb Cortex. 2019;29: 875–891. doi:10.1093/cercor/bhy291

43. Kohl C, Parviainen T, Jones SR. Neural Mechanisms Underlying Human Auditory Evoked Responses Revealed By Human Neocortical Neurosolver. Brain Topogr. 2022;35: 19–35. doi:10.1007/s10548-021-00838-0

44. Hodge RD, Bakken TE, Miller JA, Smith KA, Barkan ER, Graybuck LT, et al. Conserved cell types with divergent features in human versus mouse cortex. Nature. 2019;573: 61–68. doi:10.1038/s41586-019-1506-7

45. Molnár G, Oláh S, Komlósi G, Füle M, Szabadics J, Varga C, et al. Complex Events Initiated by Individual Spikes in the Human Cerebral Cortex. PLoS Biol. 2008;6: e222. doi:10.1371/journal.pbio.0060222

46. Oláh S, Komlósi G, Szabadics J, Varga C, Tóth É, Barzó P, et al. Output of neurogliaform cells to various neuron types in the human and rat cerebral cortex. Front Neural Circuits. 2007;1. Available: https://www.frontiersin.org/articles/10.3389/neuro.04.004.2007

47. Yáñez IB, Muñoz A, Contreras J, Gonzalez J, Rodriguez-Veiga E, DeFelipe J. Double bouquet cell in the human cerebral cortex and a comparison with other mammals. J Comp Neurol. 2005;486: 344–360. doi:10.1002/cne.20533

48. Komlósi G, Molnár G, Rózsa M, Oláh S, Barzó P, Tamás G. Fluoxetine (Prozac) and Serotonin Act on Excitatory Synaptic Transmission to Suppress Single Layer 2/3 Pyramidal Neuron-Triggered Cell Assemblies in the Human Prefrontal Cortex. J Neurosci. 2012;32: 16369–16378. doi:10.1523/JNEUROSCI.2618-12.2012

49. Molnár G, Rózsa M, Baka J, Holderith N, Barzó P, Nusser Z, et al. Human pyramidal to interneuron synapses are mediated by multi-vesicular release and multiple docked vesicles. eLife. 5: e18167. doi:10.7554/eLife.18167

50. Obermayer J, Heistek TS, Kerkhofs A, Goriounova NA, Kroon T, Baayen JC, et al. Lateral inhibition by Martinotti interneurons is facilitated by cholinergic inputs in human and mouse neocortex. Nat Commun. 2018;9: 4101. doi:10.1038/s41467-018-06628-w

51. Seeman SC, Campagnola L, Davoudian PA, Hoggarth A, Hage TA, Bosma-Moody A, et al. Sparse recurrent excitatory connectivity in the microcircuit of the adult mouse and human cortex. Slutsky I, Marder E, Sjöström PJ, editors. eLife. 2018;7: e37349. doi:10.7554/eLife.37349

52. Gidon A, Zolnik TA, Fidzinski P, Bolduan F, Papoutsi A, Poirazi P, et al. Dendritic action potentials and computation in human layer 2/3 cortical neurons. Science. 2020;367: 83–87. doi:10.1126/science.aax6239

53. Mohan H, Verhoog MB, Doreswamy KK, Eyal G, Aardse R, Lodder BN, et al. Dendritic and Axonal Architecture of Individual Pyramidal Neurons across Layers of Adult Human Neocortex. Cereb Cortex N Y N 1991. 2015;25: 4839–4853. doi:10.1093/cercor/bhv188

54. Chameh HM, Rich S, Wang L, Chen F-D, Zhang L, Carlen PL, et al. Sag currents are a major contributor to human pyramidal cell intrinsic differences across cortical layers. bioRxiv; 2020. p. 748988. doi:10.1101/748988

55. Yao HK, Guet-McCreight A, Mazza F, Chameh HM, Prevot TD, Griffiths J, et al. Reduced inhibition in depression impairs stimulus processing in human cortical microcircuits. bioRxiv; 2021. p. 2021.02.17.431698. doi:10.1101/2021.02.17.431698

56. Guet-McCreight A, Chameh HM, Mahallati S, Wishart M, Tripathy SJ, Valiante TA, et al. Age-dependent increased sag amplitude in human pyramidal neurons dampens baseline cortical activity. Cereb Cortex. 2022; bhac348. doi:10.1093/cercor/bhac348

57. Mazza F, Valiante TA, Griffiths JD, Hay E. EEG biomarkers of reduced inhibition in human cortical microcircuits in depression. Neuroscience; 2021 Jul. doi:10.1101/2021.07.18.452836

58. Hagen E, Næss S, Ness TV, Einevoll GT. Multimodal modeling of neural network activity: computing LFP, ECoG, EEG and MEG signals with LFPy2.0. bioRxiv; 2018. p. 281717. doi:10.1101/281717

59. Arber C, Li M. Cortical interneurons from human pluripotent stem cells: prospects for neurological and psychiatric disease. Front Cell Neurosci. 2013;7. Available: https://www.frontiersin.org/articles/10.3389/fncel.2013.00010

60. Krienen FM, Goldman M, Zhang Q, C H Del Rosario R, Florio M, Machold R, et al. Innovations present in the primate interneuron repertoire. Nature. 2020;586: 262–269. doi:10.1038/s41586-020-2781-z

61. Carnevale NT, Hines ML. The NEURON Book. Cambridge: Cambridge University Press; 2006. doi:10.1017/CBO9780511541612

62. Loken C, Gruner D, Groer L, Peltier R, Bunn N, Craig M, et al. SciNet: Lessons Learned from Building a Power-efficient Top-20 System and Data Centre. J Phys Conf Ser. 2010;256: 012026. doi:10.1088/1742-6596/256/1/012026

63. Ponce M, van Zon R, Northrup S, Gruner D, Chen J, Ertinaz F, et al. Deploying a Top-100 Supercomputer for Large Parallel Workloads: the Niagara Supercomputer. Proceedings of the Practice and Experience in Advanced Research Computing on Rise of the Machines (learning). Chicago IL USA: ACM; 2019. pp. 1–8. doi:10.1145/3332186.3332195

64. Teleńczuk B, Dehghani N, Le Van Quyen M, Cash SS, Halgren E, Hatsopoulos NG, et al. Local field potentials primarily reflect inhibitory neuron activity in human and monkey cortex. Sci Rep. 2017;7: 40211. doi:10.1038/srep40211

65. Gentet LJ, Kremer Y, Taniguchi H, Huang ZJ, Staiger JF, Petersen CCH. Unique functional properties of somatostatin-expressing GABAergic neurons in mouse barrel cortex. Nat Neurosci. 2012;15: 607–612. doi:10.1038/nn.3051

66. Destexhe A, Rudolph M, Fellous JM, Sejnowski TJ. Fluctuating synaptic conductances recreate in vivo-like activity in neocortical neurons. Neuroscience. 2001;107: 13–24. doi:10.1016/s0306-4522(01)00344-x

67. McCann H, Pisano G, Beltrachini L. Variation in Reported Human Head Tissue Electrical Conductivity Values. Brain Topogr. 2019;32: 825–858. doi:10.1007/s10548-019-00710-2

68. Welch P. The use of fast Fourier transform for the estimation of power spectra: A method based on time averaging over short, modified periodograms. IEEE Trans Audio Electroacoustics. 1967;15: 70–73. doi:10.1109/TAU.1967.1161901

69. Donoghue T, Haller M, Peterson EJ, Varma P, Sebastian P, Gao R, et al. Parameterizing neural power spectra into periodic and aperiodic components. Nat Neurosci. 2020;23: 1655–1665. doi:10.1038/s41593-020-00744-x

70. Koshiyama D, Kirihara K, Tada M, Nagai T, Fujioka M, Usui K, et al. Reduced Auditory Mismatch Negativity Reflects Impaired Deviance Detection in Schizophrenia. Schizophr Bull. 2020;46: 937–946. doi:10.1093/schbul/sbaa006

71. Bodatsch M, Ruhrmann S, Wagner M, Müller R, Schultze-Lutter F, Frommann I, et al. Prediction of Psychosis by Mismatch Negativity. Biol Psychiatry. 2011;69: 959–966. doi:10.1016/j.biopsych.2010.09.057

72. Lodge DJ, Behrens MM, Grace AA. A Loss of Parvalbumin-Containing Interneurons Is Associated with Diminished Oscillatory Activity in an Animal Model of Schizophrenia. J Neurosci. 2009;29: 2344–2354. doi:10.1523/JNEUROSCI.5419-08.2009

73. Umbricht D, Schmid L, Koller R, Vollenweider FX, Hell D, Javitt DC. Ketamine-induced deficits in auditory and visual context-dependent processing in healthy volunteers: implications for models of cognitive deficits in schizophrenia. Arch Gen Psychiatry. 2000;57: 1139–1147. doi:10.1001/archpsyc.57.12.1139

74. Krystal JH, Karper LP, Seibyl JP, Freeman GK, Delaney R, Bremner JD, et al. Subanesthetic Effects of the Noncompetitive NMDA Antagonist, Ketamine, in Humans: Psychotomimetic, Perceptual, Cognitive, and Neuroendocrine Responses. Arch Gen Psychiatry. 1994;51: 199–214. doi:10.1001/archpsyc.1994.03950030035004

75. Lepock JR, Ahmed S, Mizrahi R, Gerritsen CJ, Maheandiran M, Drvaric L, et al. Relationships between cognitive event-related brain potential measures in patients at clinical high risk for psychosis. Schizophr Res. 2020;226: 84–94. doi:10.1016/j.schres.2019.01.014

76. Silberberg G, Markram H. Disynaptic inhibition between neocortical pyramidal cells mediated by Martinotti cells. Neuron. 2007;53: 735–746. doi:10.1016/j.neuron.2007.02.012

77. Næss S, Halnes G, Hagen E, Hagler DJ, Dale AM, Einevoll GT, et al. Biophysically detailed forward modeling of the neural origin of EEG and MEG signals. NeuroImage. 2021;225: 117467. doi:10.1016/j.neuroimage.2020.117467

78. Resting-State Brain Activity in Schizophrenia and Major Depression: A Quantitative Meta-Analysis | Schizophrenia Bulletin | Oxford Academic. [cited 28 Mar 2023]. Available: https://academic.oup.com/schizophreniabulletin/article/39/2/358/1824284?login=false

79. Molina V, Bachiller A, Suazo V, Lubeiro A, Poza J, Hornero R. Noise power associated with decreased task-induced variability of brain electrical activity in schizophrenia. Eur Arch Psychiatry Clin Neurosci. 2016;266: 55–61. doi:10.1007/s00406-014-0569-6

80. Knyazeva MG, Jalili M, Meuli R, Hasler M, De Feo O, Do KQ. Alpha rhythm and hypofrontality in schizophrenia. Acta Psychiatr Scand. 2008;118: 188–199. doi:10.1111/j.1600-0447.2008.01227.x

81. Swann N, Tandon N, Canolty R, Ellmore TM, McEvoy LK, Dreyer S, et al. Intracranial EEG Reveals a Time- and Frequency-Specific Role for the Right Inferior Frontal Gyrus and Primary Motor Cortex in Stopping Initiated Responses. J Neurosci. 2009;29: 12675–12685. doi:10.1523/JNEUROSCI.3359-09.2009

82. Ruiz MH, Strübing F, Jabusch H-C, Altenmüller E. EEG oscillatory patterns are associated with error prediction during music performance and are altered in musician's dystonia. NeuroImage. 2011;55: 1791–1803. doi:10.1016/j.neuroimage.2010.12.050

83. Wessel JR, Conner CR, Aron AR, Tandon N. Chronometric Electrical Stimulation of Right Inferior Frontal Cortex Increases Motor Braking. J Neurosci. 2013;33: 19611–19619. doi:10.1523/JNEUROSCI.3468-13.2013

84. Lundqvist M, Rose J, Herman P, Brincat SL, Buschman TJ, Miller EK. Gamma and Beta Bursts Underlie Working Memory. Neuron. 2016;90: 152–164. doi:10.1016/j.neuron.2016.02.028

85. Miller EK, Lundqvist M, Bastos AM. Working Memory 2.0. Neuron. 2018;100: 463–475. doi:10.1016/j.neuron.2018.09.023

86. Hanslmayr S, Matuschek J, Fellner M-C. Entrainment of prefrontal beta oscillations induces an endogenous echo and impairs memory formation. Curr Biol CB. 2014;24: 904–909. doi:10.1016/j.cub.2014.03.007

87. Zavala BA, Jang AI, Zaghloul KA. Human subthalamic nucleus activity during non-motor decision making. eLife. 2017;6: e31007. doi:10.7554/eLife.31007

88. Newson JJ, Thiagarajan TC. EEG Frequency Bands in Psychiatric Disorders: A Review of Resting State Studies. Front Hum Neurosci. 2019;12. Available: https://www.frontiersin.org/articles/10.3389/fnhum.2018.00521

89. Van Derveer AB, Bastos G, Ferrell AD, Gallimore CG, Greene ML, Holmes JT, et al. A Role for Somatostatin-Positive Interneurons in Neuro-Oscillatory and Information Processing Deficits in Schizophrenia. Schizophr Bull. 2021;47: 1385–1398. doi:10.1093/schbul/sbaa184

90. Guet-McCreight A, Chameh HM, Mazza F, Prevot TD, Valiante TA, Sibille E, et al. In-silico testing of new pharmacology for restoring inhibition and human cortical function in depression. bioRxiv; 2023. p. 2023.02.22.529541. doi:10.1101/2023.02.22.529541

91. Murakami S, Okada Y. Contributions of principal neocortical neurons to magnetoencephalography and electroencephalography signals. J Physiol. 2006;575: 925–936. doi:10.1113/jphysiol.2006.105379

92. Jones SR, Pritchett DL, Sikora MA, Stufflebeam SM, Hämäläinen M, Moore CI. Quantitative analysis and biophysically realistic neural modeling of the MEG mu rhythm: rhythmogenesis and modulation of sensory-evoked responses. J Neurophysiol. 2009;102: 3554–3572. doi:10.1152/jn.00535.2009

93. Volman V, Behrens MM, Sejnowski TJ. Downregulation of Parvalbumin at Cortical GABA Synapses Reduces Network Gamma Oscillatory Activity. J Neurosci. 2011;31: 18137–18148. doi:10.1523/JNEUROSCI.3041-11.2011

94. Scheuer T, dem Brinke E auf, Grosser S, Wolf SA, Mattei D, Sharkovska Y, et al. Reduction of cortical parvalbumin-expressing GABAergic interneurons in a rodent hyperoxia model of preterm birth brain injury with deficits in social behavior and cognition. Development. 2021;148: dev198390. doi:10.1242/dev.198390

95. Kang HJ, Voleti B, Hajszan T, Rajkowska G, Stockmeier CA, Licznerski P, et al. Decreased expression of synapse-related genes and loss of synapses in major depressive disorder. Nat Med. 2012;18: 1413–1417. doi:10.1038/nm.2886

96. Douglas RJ, Martin KAC. Neuronal circuits of the neocortex. Annu Rev Neurosci. 2004;27: 419–451. doi:10.1146/annurev.neuro.27.070203.144152

97. Casado-Román L, Carbajal GV, Pérez-González D, Malmierca MS. Prediction error signaling explains neuronal mismatch responses in the medial prefrontal cortex. PLOS Biol. 2020;18: e3001019. doi:10.1371/journal.pbio.3001019